nature physics

ARTICLES

https://doi.org/10.1038/s41567-022-01517-y

Quantum logic detection of collisions between single atom–ion pairs

Or Katz[1,2] ✉, Meirav Pinkas[1], Nitzan Akerman[1] and Roee Ozeri[1]

Studies of interactions between a single pair of atoms in a quantum state are a corner-stone of quantum chemistry, yet the number of demonstrated techniques that enable the observation and control of the outcome of a single collision is still small. Here we demonstrate a technique to study interactions between an ultracold neutral atom and a cold ion using quantum logic. We measure the inelastic release of hyperfine energy in a collision between an ultracold rubidium atom and isotopes of singly ionized strontium that we do not have experimental control over. We detect the collision outcome and measure the inelastic rate of the chemistry ion by reading the motional state of a logic ion qubit in a single shot. Our work extends the toolbox for studying elastic, inelastic and reactive chemical processes with existing experimental tools, especially for atomic and molecular ions for which direct laser cooling and state detection are unavailable.

Inelastic processes have long captured great scientific and applicable interest. When two atoms are brought into close proximity, they can change their physical state and convert their internal energy into an increase or decrease in their kinetic energy. Traditionally, these processes are studied by measuring variations in average thermodynamic properties such as the temperature, energy and pressure of macroscopic samples comprising many atoms.

At the microscopic scale, the dynamics and outcome of such processes are governed by the rules of quantum mechanics. Short-range chemical forces typically produce many-body correlations in the electronic state of the atoms that comprise a molecular complex[1]. As modest molecular complexes typically consist of tens to hundreds of electrons, and as the necessary computing power for an exact ab initio computation scales exponentially with the number of electrons, accurate calculation of a single collision outcome remains a great computational challenge[2,3]. Consequently, accurate theoretical modelling often requires an experimental calibration of several free parameters.

The advent of ultracold atomic gases enabled the study of collisions in the ultracold regime between neutral atoms. In these systems, resonant scattering phenomena such as Feshbach and shape resonances enable coherent and efficient interactions between atoms[4,5], as well as the precise experimental calibration of the molecular potentials.

Hybrid systems of laser-cooled trapped ions and ultracold neutral atoms offer pristine experimental tools for the study of collisions of a single ion–atom pair[6,7]. These systems enable us to explore cold collisions as ions can be laser cooled near their motional ground state and atoms to temperatures below the millikelvin range. Various inelastic processes were studied with these systems including spin exchange[8–11], spin relaxation[12], charge exchange[13–17], excitation exchange[18], molecular association and dissociation[19,20] and elastic processes[21,22]. Although hybrid atom–ion systems provide exquisite control over the physical state of both the atom and the ion, the necessary degree of control in their preparation and detection often severely limits the range of investigated atomic and molecular species, as well as the internal states involved.

Quantum logic techniques can alleviate these experimental limitations, and enable the preparation and measurement of atomic and molecular species to which access is inefficient or challenging[23]. These methods are widely applied in spectroscopy of atoms and molecules[24–27], in precision measurements[28,29] in quantum information[30] and in search of new physics beyond the standard model[31]. For trapped ion systems, a typical realization consists of a pair of different species, whose motion is coupled by the strong coulomb force. The transitions of one (spectroscopy) ion are investigated by coupling their optical properties with the collective motion of the crystal (for example, by sideband transitions[23] or via multiple photon recoils[32,33]). The other (logic) ion qubit can be initialized, manipulated and detected by optical means. Quantum logic is manifested in the mapping of the motional state of the crystal onto the quantum state of the logic ion qubit, thus enabling the deduction of whether the spectroscopy ion has or has not undergone a transition when interacting with light.

Several works employed or proposed elements of quantum logic to detect and study collisions. Charge exchange rates between an ensemble of molecular ions and an ensemble of ultracold atoms were measured using sympathetic cooling and logic mass spectroscopy via co-trapped ions[34]. Another study traced the molecular association of a single cold molecular ion with a room-temperature gas using quantum logic[35]. Other recent works suggested using a variation of quantum logic for coherent manipulation of the molecule using phonon resolved transitions[36], and studying the Al^+ optical clock transition during its interaction with ultracold atoms[37]. Quantum logic has not yet been applied to measure the inelastic processes of a single pair of cold atoms that are optically inaccessible.

Here we present and experimentally demonstrate a quantum logic method to study elastic, inelastic and reactive processes of a single pair of atoms. Our technique enables us to measure inelastic collision of a chemistry ion in a single shot with high efficiency via its effect on the motion of another logic ion. We demonstrate the technique via measurement of cold hyperfine-changing exothermic collisions between a ^{87}Rb atom and a singly ionized Sr ion. We explore the interaction for all four stable isotopes ($^{84}Sr^+$, $^{86}Sr^+$, $^{87}Sr^+$ and $^{88}Sr^+$) as a chemistry ion using additional $^{88}Sr^+$ as a logic ion. This method opens new avenues for the study of quantum chemistry, with potential applications in measuring reaction cross-sections,

[1]Department of Physics of Complex Systems, Weizmann Institute of Science, Rehovot, Israel. [2]Present address: Department of Electrical and Computer Engineering, Duke University, Durham, NC, USA. ✉e-mail: or.katz@duke.edu

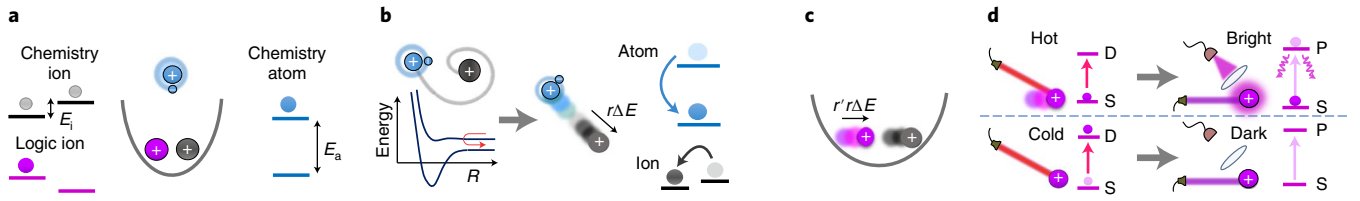

Fig. 1 | Logic detection of exothermic processes. a, State initialization. The system consists of three bodies: a logic ion co-trapped with a chemistry ion, and a free neutral atom or molecule with which the chemistry ion interacts. The motional and internal states of the logic ion and the atoms can be initialized and coherently controlled (for example via cooling and optical pumping). **b**, Atom–ion collision. Long-range attraction forces lead to spiralling of the atom and chemistry ion, resulting in a cold Langevin collision. The state of the chemistry ion following the collision is determined by the short-range interaction with the atom. In exothermic collisions, scattering between molecular potentials results in a decrease in the total internal energy (for example $\Delta E = E_a + E_i$) and an increase in the kinetic energy of the colliding bodies. Here, the chemistry ion gains a fraction $r = m_a/(m_a + m_i)$ of that energy. The effect of the presence of the logic ion on the atom–chemistry ion scattering is negligible. **c**, Sympathetic heating. Strong Coulomb forces between the two ions correlate their motion, as they share the same phononic modes of the trap. The kinetic energy of the chemistry ion is consequently distributed between these modes. For near-equal ion masses the energy is approximately equally distributed on average, such that each mode gains $r' \approx 1/6$ of the energy. **d**, Logic detection of motion. The occurrence of an inelastic collision is detected through the motional state of the logic ion. Different states of motion (hot/cold) of the crystal are mapped onto different internal states of the logic ion qubit (for example *S* or *D* electronically excited states) that are detected via state-selective fluorescence (bright or dark).

quantum resonances, collisional cooling of atoms and molecules, and reactions dynamics of optically inaccessible reactants.

Results

Quantum logic technique. To describe the quantum logic technique, we consider a two-ion crystal composed of a logic ion that can be manipulated and detected efficiently, and a chemistry ion whose interaction with background atoms we would like to study. Our method is applicable to the study of processes in which energy is released to, or removed from, the motion of the colliding bodies. We focused our analysis on exothermic processes and analysed logic detection of endothermic and elastic processes in the Methods.

An exothermic process requires the collision entrance channel to be above the absolute ground state of the molecular complex. For simplicity, here we analysed the case in which the atom is initially prepared in an excited state with a non-zero internal energy $E_a > 0$, and that the chemistry ion has an internal energy E_i as presented in Fig. 1a. We assume that the internal states of the logic and neutral atoms can be efficiently initialized, that the atom is laser cooled and that the ions are trapped and cooled near the motional ground state.

When the neutral atom approaches the chemistry ion at a distance R, it is attracted by its polarization potential $-1/R^4$, and spirals inwards towards a short-range (Langevin) collision[38] as shown in Fig. 1b. During the collision, short-range chemical forces that are specific to the interacting atom–ion pair correlate the quantum state of the complex on different molecular potential energy curves[39]. For the current discussion, we assumed that the molecular complex dissociates following the collision. The final state of the colliding parties depends on their initial states and on the amplitudes of the scattering matrix characterizing the collision. As energy is conserved, the internal energy difference between the initial and final states of the colliding atoms, $\Delta E = E_a \pm E_i$, is converted into kinetic energy. In the centre-of-mass frame an energy of $r\Delta E$ is released into the kinetic motion of the chemistry ion, where $r = m_a/(m_a + m_i)$, and m_a and m_i are the masses of the chemistry atom and ion respectively.

The energy release into the motion of the chemistry ion sympathetically stimulates the motion of the mutually trapped logic ion, as shown in Fig. 1c. The energy is distributed between the six motional modes of the trap almost equally for ions with similar masses. Detection of the motion of the logic ion can be realized via various optical thermometry techniques that rely on state-dependent fluorescence and the Doppler effect[7,40]. The particular detection technique realized in our experiment and shown in Fig. 1d enables single-shot detection of the inelastic collision using electron shelving as outlined below.

Experimental implementation. The experimental set-up consisted of a mixture of laser-cooled atoms and electrically trapped ions[7], as shown schematically in Fig. 2a. We used a magneto-optical trap to laser cool and collect a cloud of 10^6 ^{87}Rb atoms that were efficiently loaded into an off-resonant optical lattice. An absorption image of the trapped atoms is shown in Fig. 2b. We controlled the internal spin state of the atoms in the ground state, $|F, M\rangle_{Rb}$, using a sequence of microwave and optical pumping pulses. We then shuttled the cloud to the lower vacuum chamber by varying the relative optical frequencies of two counter-propagating optical lattice beams. The quantum numbers of the total atomic spin of the rubidium atoms and their projection along the magnetic field axis are F and M respectively.

In addition, we trapped a two-ion crystal in a linear Paul trap located in the lower vacuum chamber. The crystal is composed of $^{88}Sr^+$ as the logic ion (purple) and one of the stable isotopes $^{84}Sr^+$, $^{86}Sr^+$, $^{87}Sr^+$ or $^{88}Sr^+$ as the chemistry ion (black). We realized isotope-selective loading via frequency tuning of the photo-ionizing laser. In Fig. 2c we present fluorescence imaging of the two ions, where the bright logic ion efficiently scatters photons of the detection laser, whereas the chemistry ion ($^{86}Sr^+$), is considerably off-resonant and therefore does not appear. We identified the isotope of the chemistry ion via mass spectrometry[41] as shown in Fig. 2d. Here, we applied resonant electric fields ('tickle') that heated the mass-dependent axial motional mode of the crystal, and monitored the resulting decrease in the fluorescence of the logic ion due to heating. Further details of the neutral atom apparatus are given in Supplementary Note 1 and details of the ion set-up are provided in Supplementary Note 2.

During the shuttling of atoms towards the lower chamber, the logic ion was laser cooled to close to its ground motional state via sideband cooling, and its spin was optically pumped. The chemistry ion was sympathetically cooled to near its motional ground state by its Coulomb interaction with the laser-cooled logic ion, and its spin state was driven into a mixed state by sporadic absorption of off-resonant photons. As the sparse atomic cloud traversed through the ion trap, the atoms can be captured by the attractive long-range polarization potential of one of the two ions into a collision. To study the effect of single collision events, we set the probability of Langevin-type collisions of each ion per atomic cloud passage to be relatively small (about 30%) by controlling the cloud velocity and the loading time of the magneto-optical trap.

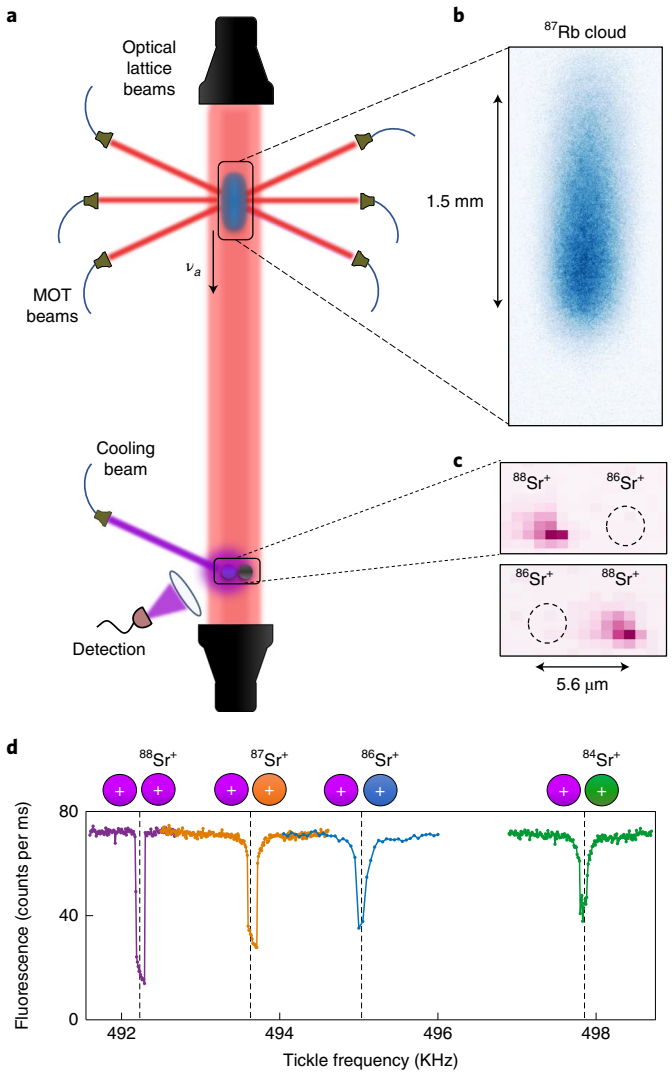

Fig. 2 | Experimental set-up. a, Set-up schematics. A cloud of neutral atoms is laser cooled and loaded into an off-resonant optical dipole trap. A pair of ions is loaded in a linear Paul trap and cooled to near the ground state. The dilute atomic cloud is optically shuttled across the ions in the trap at velocity v_a, and during its passage, a spiralling collision between one atom in the cloud and one of the ions can occur. MOT, magneto-optical trap. **b**, Absorption imaging of the atomic cloud in the top chamber. **c**, Fluorescence imaging of a two-ion crystal composed of a logic ion ($^{88}Sr^+$) and a chemistry ion ($^{86}Sr^+$), which is always dark. The two orderings of the two-ion crystal are shown to exemplify the presence of the dark ion. **d**, Verification of the chemistry ion isotope. We selectively loaded a particular isotope, and verified its mass by measuring the resonance frequency of the centre-of-mass mode. The latter is inferred from the decrease in the logic ion's fluorescence to resonance with a time-dependent external electric field (tickle). Dashed lines mark the analytically calculated frequencies of the different ion pairs by equation (7) in the Methods.

Hyperfine-changing collisions. At the onset of a collision, the spin-dependent scattering channels of the atom–ion complex are dominated by the bare atomic states, determined by the atomic hyperfine coupling to nuclear spins and Zeeman coupling to the magnetic field. For ^{87}Rb, the coupling of the electron to the 3/2 spin in its nucleus sets a large frequency gap between the lower ($F=1$) and upper ($F=2$) hyperfine manifolds of about 6.8 GHz (that is, an energy gap of $E_a = k_B \times (328\,\mathrm{mK})$ where k_B is the Boltzmann constant), whereas even isotopes of Sr^+ have zero nuclear spin and their Zeeman magnetic splitting in the experiment is small ($E_i < k_B \times 1\,\mathrm{mK}$). As the atoms spiral inwards to short distances, the two valence electrons of the atom–ion complex experience spin-dependent molecular interaction. The dominant short-range interactions in our experiment were spin exchange, corresponding to the singlet and triplet molecular curves, and weaker spin relaxation that coupled the electronic spins to the orbital angular momentum of the complex. Both interactions can mix the spin channels of the isolated atoms, and alter their initial spin state after scattering.

In this work we focused on hyperfine-changing collisions, in which the rubidium, initially in one of the $|F=2, M\rangle$ states, is scattered to the $F=1$ manifold. As the mass of rubidium and strontium is nearly equal ($r \approx 1/2$), the chemistry ion typically gains half of the internal energy $k_B \times (164\,\mathrm{mK})$. This energy is distributed between the phononic modes of the two-ion crystal, heating each mode by $k_B \times (27\,\mathrm{mK})$ on average, thus setting the logic ion in motion.

Logic detection. To characterize the inelastic rate, we measured the occurrence probability of a single hyperfine-changing collision by detecting the change in motion of the logic ion.

Various ion thermometry techniques have been developed to characterize and detect the motion of trapped ions. Sideband and carrier Rabi thermometry are mostly sensitive at low ion temperatures below a few millikelvin per mode, whereas Doppler cooling thermometry is mostly sensitive at temperatures above hundreds of millikelvin per mode[7]. However, these techniques are relatively inefficient at single-shot detection of motion of tens of millikelvin per mode, as occurs in heating by a single hyperfine-changing collision. Here we realized and numerically characterized a different coherent electron-shelving technique, which maps a hot ion qubit to the S ground state but shelves a cold ion qubit to the D electronically excited state.

Our method uses the following operations after the interaction of the ions with the atomic cloud. First, we applied optical pumping pulses to initialize the logic ion in a particular spin state to enable the detection of its motion irrespective of its spin state. Then, we applied two π pulses of narrow-band 674 nm light, tuned on resonance with the carrier of two different optical transitions between the $S_{1/2}$ and the $D_{5/2}$ manifolds, as shown in Fig. 1d for a single transition. When the ion was cold and in the absence of collisions, we succeeded in transferring it to the D state with above 99% fidelity. In contrast, when the logic ion was heated, it oscillated in the trap with large amplitude and modulated its position with respect to the optical wavefront of the shelving beam. The periodic motion compromised the coherent shelving operation, lowered its success probability and thus left a hot ion in the S state. We then discriminated between the hot (S) and cold (D) ion cases by state-selective fluorescence on the $S_{1/2} \rightarrow P_{1/2}$ strong dipole transition. Numerical characterization of this shelving technique and extensions to other configurations are presented in the Methods and in Extended Data Fig. 1.

Rate measurements. In Fig. 3 we present the probability that the logic ion appeared bright (P_{bright}) after the atomic cloud passage. To characterize and account for direct heating of the logic ion by collisions, we first characterized collisions of ^{87}Rb in the $F=2$ manifold with a crystal of two $^{88}Sr^+$ ions whose spins were initialized either in $|\downarrow\downarrow\rangle$ (Fig. 3a) or $|\uparrow\uparrow\rangle$ (Fig. 3b). As both ions could be efficiently detected, we characterized the probability of the two ions appearing bright as p_2 and the probability that only a single ion appeared bright as p_1. The results presented exclude the effect of technical errors and micromotion-induced heating[38,42] by subtracting the small probability that the ion appears bright when the experiment is repeated with the Rb cloud in $F=1$ (Methods). Therefore, all bright

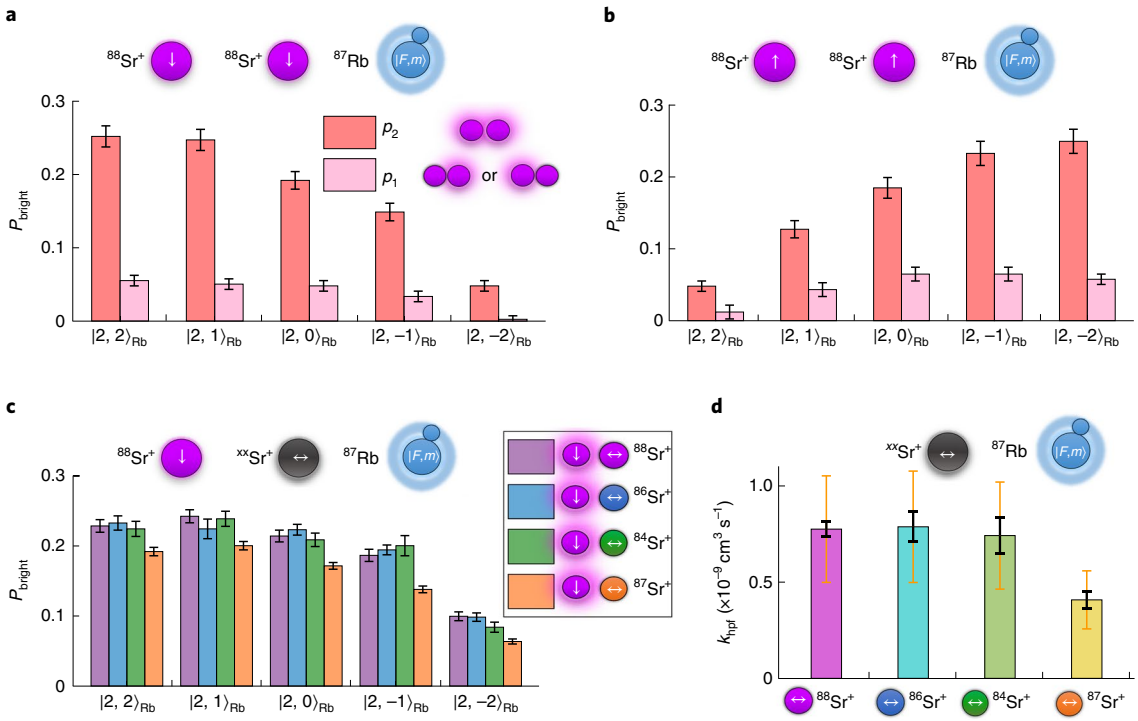

Fig. 3 | Logic detection of hyperfine-changing collisions. a,**b**, Probability of measuring a bright (hot) ion in a two-^{88}Sr$^+$-ion crystal for ions prepared with $|\downarrow\downarrow\rangle$ (**a**) or $|\uparrow\uparrow\rangle$ (**b**) spins and different internal states of the ^{87}Rb atoms. The probability of correlated events (p_2) is considerably higher than the probability of uncorrelated events (p_1), indicating high detection efficiency (about 80%) of the shelving detection. **c**, Probability of measuring a single spin-down logic ion ^{88}Sr$^+$ bright, and any of the isotopes of Sr$^+$ as chemistry ion is in a spin-unpolarized state, symmetric to up and down permutations. The statistics include collisions of an atom with the chemistry ion or with the logic ion. **d**, The hyperfine-changing rate of the different isotopes. We quantified the inelastic rate of the atom and the chemistry ion by subtracting from **c** the collision probability of the logic ion from **a**, normalizing by the detection efficiency, and averaging over the Rb internal states. Black bars represent the relative uncertainty between the isotopes, and orange bars represent the global uncertainty on the absolute rate, which is higher due to uncertainty of the Langevin rate. Data in **a**–**c** exclude small detection errors and stray heating not associated with hyperfine-changing collisions, see Methods. Bars in **a**–**c** represent 1σ binomial uncertainties.

events in Fig. 3 are associated with hyperfine-changing collisions with the Rb atom.

It is apparent that collisions in which the atomic and ion spins are anti-parallel are more probable, and that the brightness of the two ^{88}Sr$^+$ ions is correlated ($p_2 > p_1$). The former observation agrees with the dominance of the spin-exchange interaction between Sr$^+$ and Rb, whereas the latter is associated with the strong sympathetic heating of the ions and the relatively high detection efficiency of our scheme $\eta = p_2/(p_1+p_2) \approx 0.8$.

In Fig. 3c we present the brightness of the logic ion for each of the three isotopes ^{84}Sr$^+$, ^{86}Sr$^+$ and ^{87}Sr$^+$ when the logic ion was prepared in $|\downarrow\downarrow\rangle$. The linear polarization and unresolved spectrum of the cooling light in our experiment rendered the initial spin distribution of the chemistry ion to be symmetric for up and down permutations (that is spin unpolarized), denoted $\leftrightarrow$. As ^{84}Sr$^+$ and ^{86}Sr$^+$ have two spin states in their electronic ground state, they were initialized in a completely mixed spin state whose density matrix is $(|\uparrow\rangle\langle\uparrow| + |\downarrow\rangle\langle\downarrow|)/2$ but ^{87}Sr$^+$ has a nuclear spin $I = 9/2$, and therefore multiple spin states. We estimated that it was optically pumped to its lower $F = 5$ hyperfine manifold due to residual scattering of the logic ion's cooling light, and was also symmetric to spin up/down permutations. We also present the case of one of the ^{88}Sr$^+$ ions being in a completely mixed spin state, constructed from the data in Fig. 3a,b as detailed in Methods. The notable decrease in the hyperfine-changing probability for decreasing values of M is a result of the spin-down orientation of the logic ion.

The logic technique enabled accurate comparison of inelastic processes between different scattering channels and between different species. In Fig. 3d we present the inelastic hyperfine-changing rate of the chemistry ion, averaged over the five magnetic states of the Rb atoms in $F = 2$ after subtracting the probability of a hyperfine-changing collision of the atom with the logic ion. Determination of the absolute scale of the rate, however, requires additional calibration of the probability of a Langevin collision. We used the calibration of ref. [9] to determine this scaling. Owing to the uncertainty of this scaling, the absolute uncertainty of the rate coefficient (orange) is greater than the relative uncertainty of the logic measurement (black) (see Methods for further details). It is evident that the even isotopes have similar hyperfine-changing rate coefficients, whereas the odd isotope, ^{87}Sr$^+$, has a rate that is almost two times smaller.

Discussion

The measured hyperfine-changing rates can be used to calibrate ab initio calculations and determine the molecular potentials of ^{87}Rb with the different isotopes of Sr$^+$. Furthermore, previous works suggested that quantum signatures of the ultracold s wave scattering (about a hundred nanokelvin for Rb–$^+$Sr) would impact the measured rate at the millikelvin range due to a phase-locking mechanism[9,43]. The measured rates of the different isotopes, and in particular the variation between the even and odd isotopes of strontium, might provide evidence for this mechanism and unveil the ultracold regime of atom–ion interactions that is otherwise inaccessible with standard ion traps[11,38].

The presented technique could potentially be applied to various other neutral and ionic pairs of atoms or molecules to calibrate their

molecular potentials, determine cross-sections and observe quantum signatures such as Feshbach or shape-type resonances[11,44,45]. It is important to note that the logic ion is located several micrometres away from the chemistry ion and has a negligible effect on the collision process.

Our scheme could also be applied to study the sympathetic cooling of motional and internal state energies of molecules via collisions with an ultracold atomic bath. Via imprint of the motion of a logic ion, the time trajectories and inelastic pathways of quenching of rotational state can potentially be studied in a non-destructive manner, and prepare the molecules in the ground state.

Finally, the logic technique could enable the study of collisions with atomic species that lack optical transitions. One example is studying the spin-dependence of resonant charge exchange reactions between a closed-shell ion (for example $^{87}Rb^+$) and its parent atom (for example ^{87}Rb). In these reactions, the release of hyperfine energy by Rb atoms prepared in $F=2$ can be monitored via electron-shelving detection of an additional logic ion. Alternatively, transitions of Rb^+ nuclear spin between different magnetic levels through collisions with Rb atoms prepared in $F=1$ could be monitored by sideband spectroscopy of the logic ion.

Online content

Any methods, additional references, Nature Research reporting summaries, source data, extended data, supplementary information, acknowledgements, peer review information; details of author contributions and competing interests; and statements of data and code availability are available at https://doi.org/10.1038/s41567-022-01517-y.

Received: 9 August 2021; Accepted: 19 January 2022;
Published online: 21 March 2022

References

1. Szabo, A. & Ostlund, N. *Modern Quantum Chemistry* (Dover, 1996).
2. Friesner, R. A. Ab initio quantum chemistry: methodology and applications. *Proc. Natl Acad. Sci. USA* **102**, 6648–6653 (2005).
3. Abrams, D. S. & Lloyd, S. Quantum algorithm providing exponential speed increase for finding eigenvalues and eigenvectors. *Phys. Rev. Lett.* **83**, 5162 (1999).
4. Chin, C., Grimm, R., Julienne, P. S. & Tiesinga, E. Feshbach resonances in ultracold gases. *Rev. Mod. Phys.* **82**, 1225 (2010).
5. Paliwal, P. et al. Determining the nature of quantum resonances by probing elastic and reactive scattering in cold collisions. *Nat. Chem.* **13**, 94–98 (2021).
6. Tomza, M. et al. Cold hybrid ion-atom systems. *Rev. Mod. Phys.* **91**, 035001 (2019).
7. Meir, Z. et al. Experimental apparatus for overlapping a ground-state cooled ion with ultracold atoms. *J. Mod. Opt.* **65**, 501–519 (2018).
8. Sikorsky, T., Meir, Z., Ben-shlomi, R., Akerman, N. & Ozeri, R. Spin-controlled atom-ion chemistry. *Nat. Commun.* **9**, 920 (2018).
9. Sikorsky, T. et al. Phase locking between different partial waves in atom-ion spin-exchange collisions. *Phys. Rev. Lett.* **121**, 173402 (2018).
10. Major, F. G. & Dehmelt, H. G. Exchange-collision technique for the rf spectroscopy of stored ions. *Phys. Rev.* **170**, 91 (1968).
11. Feldker, T. et al. Buffer gas cooling of a trapped ion to the quantum regime. *Nat. Phys.* **16**, 413–416 (2020).
12. Tscherbul, T. V., Brumer, P. & Buchachenko, A. A. Spin-orbit interactions and quantum spin dynamics in cold ion-atom collisions. *Phys. Rev. Lett.* **117**, 143201 (2016).
13. Ratschbacher, L., Zipkes, C., Sias, C. & Köhl, M. Controlling chemical reactions of a single particle. *Nat. Phys.* **8**, 649–652 (2012).
14. Rellergert, W. G. et al. Measurement of a large chemical reaction rate between ultracold closed-shell ^{40}Ca atoms and open-shell $^{174}Yb^+$ ions held in a hybrid atom-ion trap. *Phys. Rev. Lett.* **107**, 243201 (2011).
15. Ravi, K., Lee, S., Sharma, A., Werth, G. & Rangwala, S. A. Cooling and stabilization by collisions in a mixed ion-atom system. *Nat. Commun.* **3**, 1126 (2012).
16. Li, H. et al. Photon-mediated charge-exchange reactions between ^{39}K atoms and $^{40}Ca^+$ ions in a hybrid trap. *Phys. Chem. Chem. Phys.* **22**, 10870–10881 (2020).
17. Mahdian, A., Krükow, A. & Denschlag, J. H. Direct observation of swap cooling in atom-ion collisions. *N. J. Phys.* **23**, 065008 (2021).
18. Ben-shlomi, R. et al. High-energy-resolution measurements of an ultracold-atom-ion collisional cross section. *Phys. Rev. A* **103**, 032805 (2021).
19. Hall, F. H. J., Aymar, M., Bouloufa-Maafa, N., Dulieu, O. & Willitsch, S. Light-assisted ion-neutral reactive processes in the cold regime: radiative molecule formation versus charge exchange. *Phys. Rev. Lett.* **107**, 243202 (2011).
20. Mohammadi, A. et al. Life and death of a cold $BaRb^+$ molecule inside an ultracold cloud of Rb atoms. *Phys. Rev. Res.* **3**, 013196 (2021).
21. Haze, S., Sasakawa, M., Saito, R., Nakai, R. & Mukaiyama, T. Cooling dynamics of a single trapped ion via elastic collisions with small-mass atoms. *Phys. Rev. Lett.* **120**, 043401 (2018).
22. Zipkes, C., Palzer, S., Ratschbacher, L., Sias, C. & Köhl, M. Cold heteronuclear 'atom-ion collisions'. *Phys. Rev. Lett.* **105**, 133201 (2010).
23. Schmidt, P. O. et al. Spectroscopy using quantum logic. *Science* **309**, 749–752 (2005).
24. Wolf, F. et al. Non-destructive state detection for quantum logic spectroscopy of molecular ions. *Nature* **530**, 457–460 (2016).
25. Sinhal, M., Meir, Z., Najafian, K., Hegi, G. & Willitsch, S. Quantum-nondemolition state detection and spectroscopy of single trapped molecules. *Science* **367**, 1213–1218 (2020).
26. Lin, Y., Leibrandt, D. R., Leibfried, D. & Chou, C. Quantum entanglement between an atom and a molecule. *Nature* **581**, 273–277 (2020).
27. Chou, C. W. et al. Frequency-comb spectroscopy on pure quantum states of a single molecular ion. *Science* **367**, 1458–1461 (2020).
28. Brewer, S. M. et al. $^{27}Al^+$ quantum-logic clock with a systematic uncertainty below 10^{-18}. *Phys. Rev. Lett.* **123**, 033201 (2019).
29. Gebert, F. et al. Precision isotope shift measurements in calcium ions using quantum logic detection schemes. *Phys. Rev. Lett.* **115**, 053003 (2015).
30. Kienzler, D. et al. Quantum logic spectroscopy with ions in thermal motion. *Phys. Rev. X* **10**, 021012 (2020).
31. Micke, P. et al. Coherent laser spectroscopy of highly charged ions using quantum logic. *Nature* **578**, 60–65 (2020).
32. Wan, Y. et al. Precision spectroscopy by photon-recoil signal amplification. *Nat. Commun.* **5**, 3096 (2014).
33. Gebert, F. et al. Precision isotope shift measurements in calcium ions using quantum logic detection schemes. *Phys. Rev. Lett.* **115**, 053003 (2015).
34. Hall, F. H. J. & Willitsch, S. Millikelvin reactive collisions between sympathetically cooled molecular ions and laser-cooled atoms in an ion-atom hybrid trap. *Phys. Rev. Lett.* **109**, 233202 (2012).
35. Najafian, K., Meir, Z., Sinhal, M. & Willitsch, S. Identification of molecular quantum states using phase-sensitive forces. *Nat. Commun.* **11**, 4470 (2020).
36. Meir, Z., Hegi, G., Najafian, K., Sinhala, M. & Willitsch, S. State-selective coherent motional excitation as a new approach for the manipulation, spectroscopy and state-to-state chemistry of single molecular ions. *Faraday Discuss.* **217**, 561–583 (2019).
37. Tomza, M. & Lisaj, M. Interactions and charge-transfer dynamics of an Al^+ ion immersed in ultracold Rb and Sr atoms. *Phys. Rev. A* **101**, 012705 (2020).
38. Cetina, M., Grier, A. T. & Vuletić, V. Micromotion-induced limit to atom-ion sympathetic cooling in Paul traps. *Phys. Rev. Lett.* **109**, 253201 (2012).
39. Côté, R. Ultracold hybrid atom-ion systems. *Adv. Atom. Molec. Opt. Phys.* **65**, 67–126 (2016).
40. Wesenberg, J. H. et al. Fluorescence during Doppler cooling of a single trapped atom. *Phys. Rev. A* **76**, 053416 (2007).
41. Drewsen, M., Mortensen, A., Martinussen, R., Staanum, P. & Sørensen, J. L. Nondestructive identification of cold and extremely localized single molecular ions. *Phys. Rev. Lett.* **93**, 243201 (2004).
42. Pinkas, M. et al. Effect of ion-trap parameters on energy distributions of ultra-cold atom-ion mixtures. *N. J. Phys.* **22**, 013047 (2020).
43. Côté, R. & Simbotin, I. Signature of the *s* -wave regime high above ultralow temperatures. *Phys. Rev. Lett.* **121**, 173401 (2018).
44. Tomza, M., Koch, C. P. & Moszynski, R. Cold interactions between an Yb^+ ion and a Li atom: prospects for sympathetic cooling, radiative association, and Feshbach resonances. *Phys. Rev. A* **91**, 042706 (2015).
45. Weckesser, P. et al. Observation of Feshbach resonances between a single ion and ultracold atoms. Preprint at https://arxiv.org/abs/2105.09382 (2021).

Methods

Numerical model of electron-shelving detection. The demonstrated electron-shelving technique enables the motion of the logic ion to be characterized using its coherent interaction with photons. In the presence of an optical field, the interaction Hamiltonian of the trapped ion is given by

$$H_I = \frac{1}{2}\Omega\left(\mathrm{e}^{-i\delta t}\mathrm{e}^{i\mathbf{k}\cdot\mathbf{R}}\sigma_+ + \mathrm{e}^{i\delta t}\mathrm{e}^{-i\mathbf{k}\cdot\mathbf{R}}\sigma_-\right). \quad (1)$$

Here $\sigma_- = \sigma_+^\dagger = |g\rangle\langle e|$ denotes the transition operator between a single ground state $|g\rangle$ in the $S_{1/2}$ manifold to a particular excited state $|e\rangle$ in the $D_{5/2}$ manifold. $\mathbf{k}$ denotes the wavenumber vector of the shelving beam, δ denotes the frequency detuning of the optical field from the atomic line, Ω denotes the Rabi angular frequency of the quadruple transition, and $\mathbf{R}(t)$ denotes the position of the logic ion in the trap at time t.

For a finite shelving pulse of time T starting at t_0, the state of the ion evolves by the unitary operator

$$U_I = \mathcal{T}\exp\left(-i\int_{t_0}^{t_0+T} H_I(t')dt'\right), \quad (2)$$

where $\mathcal{T}$ denotes the time-ordering operator. Notably, the ion motion renders the Hamiltonian in equation (1) non-commuting with itself at different times. For an ion initially in the ground state $|g\rangle$, we characterized the probability of measuring a bright ion (that is, in the S manifold) after a single π pulse using $P^{(1)} = |\langle g|U(T_\pi)|g\rangle|^2$, where the π pulse time $T_\pi = \pi/\Omega$ is determined by the laser power and the transition strength. In our experiment we used $T_\pi = 5\,\mu$s for the first shelving pulse and $T_\pi = 12\,\mu$s for the second. We also considered the probability of measuring a bright ion using two independent pulses $P^{(2)}$ of different transitions. Here we present the case in which the effect of each pulse is similar (that is $P^{(2)} \approx (P^{(1)})^2$), which is relevant in the experimentally realized limit of $T_\pi\omega_{z1} \gg 1$, where $\omega_{z1} = 2\pi\times 480\,$kHz is the in-phase axial motional frequency.

Between collisions, the trapped logic ion oscillates and its mean secular position follows

$$R_i(t) = \sum_{j=1}^{N_{\mathrm{ions}}} b_{ij}A_{ij}\cos(\omega_{ij}t + \phi_{ij}), \quad (3)$$

where b_{ij} are the mode participation factors of the logic ion in the chain ($|b_{ij}| = 1/\sqrt{2}$ for a two-ion crystal with nearly equal masses), $i \in \{x, y, z\}$ index the trap axes, $j \in \{1, 2\}$ index the two eigenmodes in each axis and ω_{ij} are the trap secular frequencies of motion. In our experiment the single ion trap frequencies were 0.4 MHz and 1 MHz for the radial modes. The phases of motion ϕ_{ij} were randomly distributed in every experimental realization, whereas the amplitudes A_{ij} depended on the phonon distribution in each mode.

To characterize the detection efficiency of this technique, we numerically simulated the dynamics of a trapped ion crystal following a single instantaneous collision with a cold neutral atom moving at a velocity $\boldsymbol{v}_{\mathrm{atom}}$ in the lab frame. Before and after the collision, the positions of the ions evolved according to the formula in ref. [46], taking into account both inherent and excess micromotion due to stray static fields. We assumed that a collision occurred at t_c and accounted for the effect of an exothermic collision by updating the coefficients A_{ij} and ϕ_{ij} in equation (3) to new values at t_c. The update was determined by finding the amplitudes and phases that maintained the positions $R_i(t_c)$ but varied the velocity of the colliding ion at t_c in the lab frame by

$$\boldsymbol{v}_{\mathrm{ion}} \to (1 - r + \alpha r\mathcal{R}(\varphi))(\boldsymbol{v}_{\mathrm{ion}} - \boldsymbol{v}_{\mathrm{atom}}) + v_{\mathrm{atom}}. \quad (4)$$

Here $\mu = m_a m_i/(m_a + m_i)$ is the reduced mass, $r = \mu/m_i$, $\mathcal{R}$ is the rotation matrix and φ is the scattering angle, randomly generated for Langevin-type collisions[47]. The unitless factor $\alpha = \sqrt{1 + 2r\Delta E/(m_i|\bar{v}_{\mathrm{ion}}|^2)}$ describes the increase of the ion's speed $\bar{v}_{\mathrm{ion}} \equiv r(v_{\mathrm{ion}} - v_{\mathrm{atom}})$ in the centre-of-mass frame, gaining kinetic energy via exothermic processes.

Following the collision dynamics, we calculated the detection probabilities $P^{(1)}$ and $P^{(2)}$ by numerically solving equation (2) with the discrete Suzuki–Trotter expansion. At this stage, we substituted the coherent evolution of the ions positions from equation (3) into the Hamiltonian (equation (1)) for $t_0 > t_c$, as we measured the ions many motional cycles after the collision time (experimentally waiting a few milliseconds after the cloud passage). As the exact trap frequencies are incommensurate, the stochastic timing of the collision effectively randomizes the phases ϕ_{ij} used in the detection stage at t_0. We repeated the calculations and averaged the results presented for the random collision parameters, including φ, ϕ_{ij} and A_{ij}. The latter are randomly sampled, following a thermal distribution in a harmonic trap with an average temperature of 1 mK.

Detection efficiency. The electron-shelving technique is sensitive to motion along the optical axis of the shelving beam as realized by equation (1) through the inner product between $\mathbf{k}$ and $\mathbf{R}$. The detection efficiency depends on two type of unitless parameter $\xi_{ij} = k_i|b_{ij}|A_{ij}$ and $\zeta_{ij} = \omega_{ij}T_\pi$. The parameters ζ_{ij} quantify the number of motional cycles of each mode during the π pulse time. It is notable that the variation in T_π corresponds to simultaneous changes in the pulse duration $T = T_\pi$ and the Rabi frequency $\Omega = \pi/T_\pi$ (for example, via the beam intensity) to meet the π pulse criterion. The parameters ξ_{ij} determine the modulation indices of the shelving operation for each harmonic component of the ion's secular motion in the trap. It is directly associated with the number of phonons N_{ij} in each mode (indexed by ij) and their Lamb–Dicke parameters $\eta_{ij} = k_i\sqrt{\hbar/(2m_i\omega_{ij})}$ by $\xi_{ij} = \eta_{ij}\sqrt{2N_{ij}}$.

In the regime where the ion motion is dominated by the released inelastic energy ($\alpha \gg 1$), the number of phonons in each mode $N_{ij} = \sqrt{rr'_{ij}\Delta E/(\hbar\omega_{ij})}$ depends on the coefficients $0 \le r'_{ij} \le 1$, which describe the relative distribution of the chemistry ion's energy between the motional modes of the crystal, satisfying $\sum_{ij} r'_{ij} = 1$ and yielding

$$\xi_{ij} = 2b_{ij}\eta_{ij}\sqrt{\frac{rr'_{ij}\Delta E}{\hbar\omega_{ij}}}. \quad (5)$$

For the atomic species we considered, the masses are almost equal and the energy-distribution coefficients are $r \approx 1/2$ and $\langle r'_{ij}\rangle \approx 1/6$.

We first discuss a simplified configuration in which the beam, tilted with an angle θ with respect to $\hat{z}$, is co-aligned with the chain's axis ($\theta = 0°$), and then discuss the experimentally realized configuration in which $\theta = 45°$. In Extended Data Fig. 1a, we present the numerically calculated brightness of the ion $P^{(1)}$ for $\theta = 0°$ as a function of $\langle\xi_{z1}\rangle$ and ζ_{z1} (that is, the unitless parameters associated with the in-phase axial mode) for the carrier transition ($\delta = 0$). Note that this configuration is sensitive only to $\langle\xi_{zj}\rangle$ and ζ_{zj}, where the averaged $j = 2$ coefficients are directly determined by the $j = 1$ coefficients for the two-ion crystal. With a sufficient number of motional oscillations within a π pulse, the ion appears bright for energetic collisions, whereas it is efficiently shelved to the D manifold and appears dark otherwise. In the low-laser-power limit ($\zeta_{zj} \gg 1$), the modulated spectrum of the ion is spectrally resolved, and the phase modulation manifests as a reduction of the Rabi frequency by the product of zeroth-order Bessel functions $\Pi_{ij}J_0(\xi_{ij})$ (ref. [48]), yielding the single-shelving detection probability

$$P^{(1)} = \cos^2\left(\frac{\pi}{2}\Pi_{ij}J_0(\xi_{ij})\right) \quad (6)$$

for narrow-line-width transitions. In Extended Data Fig. 1b, we present the probability of double shelving for $\theta = 45°$ as realized experimentally compared with the co-aligned case ($\theta = 0°$). It is evident that the variation of the detection probability spans over a smaller range of collision energies for non-zero θ compared to the co-aligned case. This is due to the non-zero contributions of ξ_{ij} of the radial modes in equation (6) that reduce the Rabi frequency of the hot ion. This is similar to the configuration that was used experimentally; black arrow indicates the predicted probability of detecting a single hyperfine-changing collision in the experiment.

Detection of other collisional processes. The shelving-detection method can be applied for the logical detection of various collisional process and configurations. Here we examined several processes for a single exemplary configuration for which the beam is co-linear with the trap axis ($\theta = 0°$) and the shelving beam intensity is low ($\zeta_{zj} \gg 1$). In this configuration, the detection efficiency of a single shelving pulse $P^{(1)}$ simply follows equation (6), and depends solely on two unitless parameters ξ_{z1}, ξ_{z2} given in equation (5). For mass-balanced configurations $\langle\xi_{z2}\rangle = \langle\xi_{z1}\rangle/\sqrt{3}$, the analysis reduces to a single unitless parameter ξ_{z1}.

Detection of low-energy-release processes. The energy dependence of the detection efficiency is encapsulated by the unitless parameter ξ_{z1}. Exothermic processes with low values of ΔE can be efficiently measured at other configurations if a large ξ_{z1} value is maintained by scaling some other parameters, for example the centre-of-mass trap frequency ω_{z1}. In this case, the scaling is given by $\xi_{zj} \propto \sqrt{\Delta E/\omega_{zj}^2}$, taking into account the frequency dependence of the Lamb–Dicke parameter in equation (5). Consequently, control over the axial trap frequencies (by variation of the electrostatic potential) enables the detected energy range to be scaled with quadratic sensitivity. In Extended Data Fig. 1c we verify this scaling numerically and present the single shelving-pulse detection efficiencies for three co-linear configurations with different axial trap frequencies. The blue curve configuration in Extended Data Fig. 1b is similar to the blue curve in Extended Data Fig. 1c except for the number of shelving pulses applied in the detection (that is $P^{(1)}$ instead of $P^{(2)}$). In the two additional configurations, the static potentials were reduced to decrease $\omega_{1z} \to \omega_{1z}/3$ (green) and $\omega_{1z} \to \omega_{1z}/10$ (dark blue), showing that the detection range was scaled by about one and two orders of magnitude respectively. It is evident that decreasing the axial trap frequency to about 50 KHz increases the sensitivity to exothermic processes, even those whose released energy is below $k_B \times (1\,\mathrm{mK})$.

Mass-unbalanced configurations. The method is also applicable to different mass combinations of the three bodies. Different masses act predominantly to alter ξ_{zj} via the two ratios m_i^c/m_i^L and m_a/m_i^c where m_a, m_i^c and m_i^L denote the mass of the

atom, chemistry ion and logic ion respectively. The ratio m_a/m_i^c between the atom and chemistry ion masses determines the fraction of energy $r = m_a/(m_i^c + m_a)$ that the crystal gains from the process, which hinders detection only when the atom is too light: $m_a \ll m_i^c$. In contrast, the ratio between the two ions $\mu_{cL} = m_i^c/m_i^L$ changes the motional frequencies of the crystal and the distribution of energy between the different modes. We estimated these effects by using the solution in ref. [49] for a two-ion crystal. The two axial frequencies $j = 1, 2$ are given by

$$\omega_{zj} = \omega_z \sqrt{\frac{1 + \mu_{cL} + (-1)^j \sqrt{1 - \mu_{cL} + \mu_{cL}^2}}{\mu_{cL}}} \tag{7}$$

where ω_z is the axial frequency of the logic ion absent the chemistry ion. We found the average mode distribution for the case where the logic and chemistry ions are at rest before a collision between the atom and chemistry ion, yielding $r'_{z1} = b_{z2}^2/3$ and $r'_{z2} = b_{z1}^2/3$, where the mode participation factors for the logic ion are

$$b_{z1} = \sqrt{\frac{1 - \mu_{cL} + \sqrt{1 - \mu_{cL} + \mu_{cL}^2}}{2\sqrt{1 - \mu_{cL} + \mu_{cL}^2}}}, \tag{8}$$

and $b_{z2} = \sqrt{1 - b_{z1}^2}$.

In Extended Data Fig. 1d, we show the scaling of ξ_{z1} and ξ_{z2} for two configurations with unbalanced mass ratios, and compare their scaling with respect to the mass-balanced configuration ($m_a = m_i^c = m_i^L$), whose parameters are denoted by ξ_{z1}^{bal} and ξ_{z2}^{bal}. In the top plot we vary m_a with fixed $m_i^c = m_i^L$, and in the bottom plot we vary m_i^c for a fixed m_i^L and a constant ratio $m_a = m_i^c$. It can be seen that the logic technique is near optimal for logic and chemistry ions of equal masses. For unbalanced masses, ξ_{z1} and ξ_{z2} are reduced with respect to the mass-balanced configuration, compromising the sensitivity with respect to low-energy-release processes. Nevertheless, decreasing the static potential can readily increase ξ_{z1} and ξ_{z2} and enable practical extension of the technique to mass-unbalanced configurations.

Logic detection of elastic collisions. The logic technique can also be used to detect momentum-changing collisions. Here, the overall kinetic energy of the three bodies is conserved, but the net momentum and energy of the crystal varies via exchange with the atom. Here we considered an exemplary configuration for which the crystal is cooled to the ground state but the atom is shuttled with a well-defined kinetic energy E_a, moving perpendicular to the shelving-beam axis. In this configuration, elastic scattering with either of the ions would generate motion along the chain's axis, provided that the scattering angle ϕ is non-zero. In Extended Data Fig. 1e we present the detection efficiency for a single spiralling Langevin collision (solid line) as a function of the atom's kinetic energy, using the same configuration parameters as the blue curve in Extended Data Fig. 1b,c (but no inelastic processes, setting $\Delta E = 0$). Momentum-changing collisions can be detected in a similar manner to exothermic collisions. The atom's kinetic energy is redistributed in the collision, transferring about $r^2E_a/3$ of that energy to motion of the ions along the beam, thus generating motion of the logic ion, enabling detection. Note that the exact distribution of energy between the different modes depends strongly on the atomic beam direction and moderately on the distribution of ϕ.

Logic detection of endothermic processes. The logic technique can be used to detect endothermic processes for which kinetic energy is converted to internal energy. For two-body collisions, endothermic processes with $\Delta E < 0$ can occur only if the colliding pair has sufficient initial kinetic energy. Here we considered an exemplary configuration similar to that presented in the previous section, for which a ^{87}Rb atom with kinetic energy E_a and initially in $F = 1$ collides with a chemistry Sr^+ ion, and scatters at $F = 2$. In Extended Data Fig. 1e we plot the detection efficiency (dashed line) as a function of the kinetic energy of the atoms, assuming the occurrence of a single collision hyperfine-state changing endothermic process for any $E_a > 2|\Delta E|$ (note that E_a is defined in the lab frame, hence the factor of 2). Endothermic collisions suppress elastic momentum transfer, and enable efficient logic detection of such processes following calibration of the elastic process.

Comparison with Doppler cooling thermometry. A comparison of the present detection method with monitoring of Doppler cooling curves[40] is useful, and supports its possible utilization in precision thermometry. During Doppler cooling, a hot ion scatters photons less efficiently due to the motion-induced phase modulation. Monitoring the number of scattered photons as a function of time enables the ion's temperature to be inferred. Both Doppler cooling and electron-shelving methods detect motion via the phase modulation mechanism that imparts the optical excitation of a hot ion with respect to a cold one. In the optical Bloch sphere context, the mechanism corresponds to mapping the phase of the complex Rabi frequency to the rotation axis of the atom by the beam; a cold ion has a stationary phase and a static axis whereas a hot ion with a fluctuating phase would lead to a time-varying rotation axis and inefficient transfer from the south to north poles. However, Doppler cooling thermometry is often practically limited by the photon collection efficiency of the detection method. For low collection efficiencies, observation of the motion-dependent fluorescence requires scattering of numerous photons, which in turn cool the ion and render the detection less sensitive. Consequently, the motion-dependent signal has to overcome the photon shot noise at the detection stage, often limiting the sensitivity of a single event to temperatures above 1 K (ref. [7]). In contrast, electron shelving requires absorption of a single photon to map the motional state of the ion to its electronic state, which can later be detected via fluorescence in a non-destructive manner. This method could potentially be used as thermometry and enable the detection of ΔE, for example by varying T_π or trap frequencies, and calculating the likelihood with respect to the model.

Logic detection procedure. *Subtraction of other heating effects.* Several other processes and experimental imperfections could lead to false alarms by the detection method, in which a $^{88}Sr^+$ ion is detected as bright in the absence of a hyperfine-state-changing collision. The experimental imperfections include detection errors associated with the shot noise of the detected fluorescence, as well as drifts of the shelving beam parameters. False alarms could also be generated by other atom–ion collisional processes. The finite temperature of the bodies, imperfect compensation of static electric fields (that generate excess micromotion) and micromotion-induced heating[38] can lead to failure of the shelving process due to elastic atom–ion collisions.

We performed electron-shelving detection of $^{88}Sr^+$ and recorded the probability that the ions appear bright $\tilde{P}_b(F, M)$ after passage of the Rb cloud, initialized in the state $|F, M\rangle_{Rb}$. To quantify the false alarm probability, we measured the scattering of the channels $|1, 1\rangle_{Rb}$ or $|1, -1\rangle_{Rb}$ in which hyperfine-changing collisions are suppressed due to energy conservation, except for the $^{87}Sr^+$ isotope in its upper hyperfine manifold. Importantly, as $\tilde{P}_b(F = 1, M) \ll 1$, it includes both types of false alarm, the experimental imperfections and elastic collisional processes, in an additive manner. Moreover, as $\tilde{P}_b(F, M)$ are relatively small, to leading order we could correct for the averaged false-alarm probability by directly subtracting it from the data. Specifically, the probabilities $P_{bright}(M)$ presented in Fig. 3a–c are given after the subtraction

$$P_{bright}(M) = \tilde{P}_b(2, M) - \frac{1}{2}(\tilde{P}_b(1, 1) + \tilde{P}_b(1, -1)), \tag{9}$$

for each of the M initial states of the ^{87}Rb in $F = 2$. The data for the different channels were recorded alternately to suppress potential drift and render the subtraction useful.

In Supplementary Fig. 1a–c we present the average probabilities $\tilde{P}_b(1, 1)$ and $\tilde{P}_b(1, -1)$ for the configurations associated with Fig. 3a–c respectively. In Supplementary Fig. 1a,b most reading were associated with only one of the two $^{88}Sr^+$ ions being bright at a time ($p_1 \gg p_2$), as expected from uncorrelated false alarms or low-energy changing events, and in contrast to the hyperfine-changing collisions that led to shelving failure of both ions. On average, the false-alarm probability associated with collisions with $F = 1$ atoms was about 2% per $^{88}Sr^+$ ion in all configurations in Supplementary Fig. 1a–c. For $^{87}Sr^+$ ions these results indicate that its initial state was predominantly in its lower hyperfine manifold at $F = 5$, since it has a large hyperfine splitting of about 5 GHz and collisions with $F = 1$ atoms could lead to increased heating of the crystal by changing the ion's hyperfine state. For the other isotopes, the small variations between the bars mostly indicate variation in calibrations or the long-time stability of the system. The bars for $^{84}Sr^+$ are moderately higher, probably as a result of the infrequent stray field compensation during its measurements; a consequence of its inefficient loading (see Supplementary Note 2).

Statistics for $^{88}Sr^+$ in a completely mixed state. To compare the scattering between $^{88}Sr^+$ ions and the other isotopes, in Fig. 3c we present the calculated probability P_{bright} for a configuration in which one of the two $^{88}Sr^+$ ions is polarized downwards and the second is in a completely mixed spin state denoted $\leftrightarrow$. For this purpose, we used the data in Fig. 3a,b and denote the values of the presented bars $p_{2,88}^{\downarrow\downarrow}(M)$, $p_{1,88}^{\downarrow\downarrow}(M)$ and $p_{2,88}^{\uparrow\uparrow}(M)$, $p_{1,88}^{\uparrow\uparrow}(M)$ respectively. The corresponding heating probability per ion is simply related by $p_{j,88}^{\downarrow}(M) = p_{j,88}^{\downarrow\downarrow}(M)/2$ and $p_{j,88}^{\uparrow}(M) = p_{j,88}^{\uparrow\uparrow}(M)/2$ for $j = 1, 2$. For each of the isotopes denoted by $x \in \{84, 86, 87, 88\}$ in Fig. 3c, the measured value $P_{bright}^x(M)$ can be decomposed into heating of the logic ion and heating of the chemistry ion by

$$P_{bright}^x(M) = (p_{2,88}^{\downarrow}(M) + p_{1,88}^{\downarrow}(M)) + p_{2,x}^{\leftrightarrow}(M), \tag{10}$$

where the term $p_{1,x}^{\leftrightarrow}$ is absent due to the indirect measurement of the chemistry ion. For $x \in \{84, 86, 88\}$, the completely mixed state is a 50:50 mixture of up and down spins, and therefore $p_{2,x}^{\leftrightarrow} = (p_{2,x}^{\downarrow} + p_{2,x}^{\uparrow})/2$. Using this relation, we constructed the purple bars for $^{88}Sr^+$ in Fig. 3c using $P_{bright}^{88} = \frac{3}{4}p_{2,88}^{\downarrow\downarrow} + \frac{1}{2}p_{1,88}^{\downarrow\downarrow} + \frac{1}{4}p_{2,88}^{\uparrow\uparrow}$.

Rate coefficient estimation. To estimate the rate coefficient of hyperfine-changing collisions for the different isotopes, we first determined the effective probability of a hyperfine-changing collision for a ^{87}Rb atom with a single chemistry ion (in the

absence of a logic ion). This probability, averaged over the five states of the ^{87}Rb in $F=2$ is given by

$$p^{x}_{\mathrm{hpf}} = \frac{1}{5}\sum_{M=-2}^{2}\frac{1}{\eta}\left(P^{x}_{\mathrm{bright}}(M) - (p^{\downarrow}_{2,88}(M) + p^{\downarrow}_{1,88}(M))\right),$$

where we first subtracted the contribution of inelastic heating from collisions of the logic ion with ^{87}Rb atoms, and then normalized by the detection efficiency η. The detection efficiency for the two-$^{88}Sr^{+}$-ion configuration is $\eta = p^{\leftrightarrow}_{2,88}/(p^{\leftrightarrow}_{1,88} + p^{\leftrightarrow}_{2,88})$, and it is similar for all other crystal configurations because the chemistry ion and logic ion masses are nearly equal. To convert the measured probability p^{x}_{hpf} into the rate coefficient k_{hpf}, we used the relation $k_{\mathrm{hpf}} = k_{\mathrm{L}}(p^{x}_{\mathrm{hpf}}/p_{\mathrm{L}})$ where $k_{\mathrm{L}} = 2.4\times10^{-9}\,\mathrm{cm^3\,s^{-1}}$ is the Langevin rate coefficient and p_{L} is the probability of a Langevin spiralling collision per passage of the Rb cloud. These two Langevin parameters are almost identical for all of the investigated isotopes. Hence, we can readily apply the results in ref. [9], which calibrated the Langevin ratio of a singular channel $(p^{\downarrow}_{1,88}(-2) + p^{\downarrow}_{2,88}(-2))/p_{\mathrm{L}} = 0.079 \pm 0.028$; this ratio was estimated via measurement of the energy histogram of a single ion after multiple collisions with cold ^{87}Rb prepared in $|2,-2\rangle_{\mathrm{Rb}}$. In our case, this estimation yielded a typical Langevin probability per passage centred around $p_{\mathrm{L}} \approx 0.34$, and its associated error is shown by the orange bar in Fig. 3.

Data availability

Source data are provided with this paper. Other data that support the findings of this study are available from the corresponding author on reasonable request.

References

46. Bermudez, A., Schindler, P., Monz, T., Blatt, R. & Müller, M. Micromotion-enabled improvement of quantum logic gates with trapped ions. *N. J. Phys.* **19**, 113038 (2017).
47. Zipkes, C., Ratschbacher, L., Sias, C. & Köhl, M. Kinetics of a single trapped ion in an ultracold buffer gas. *N. J. Phys.* **13**, 053020 (2011).
48. Berkeland, D. J., Miller, J. D., Bergquist, J. C., Itano, W. M. & Wineland, D. J. Minimization of ion micromotion in a Paul trap. *J. Appl. Phys.* **83**, 5025 (1998).
49. Wübbena, J. B., Amairi, S., Mandel, O. & Schmidt, P. O. Sympathetic cooling of mixed-species two-ion crystals for precision spectroscopy. *Phys. Rev. A* **85**, 043412 (2012).

Acknowledgements

We thank Z. Meir for useful comments on the manuscript. This work was supported by the Israeli Science Foundation, the Israeli Ministry of Science, Technology and Space and the Minerva Stiftung.

Author contributions

O.K., M.P., N.A. and R.O. contributed to the experimental design, construction, discussions and wrote the manuscript. O.K. collected the data and analysed the results. O.K. claims responsibility for all figures.

Competing interests

The authors declare no competing interests.

Additional information

Extended data is available for this paper at https://doi.org/10.1038/s41567-022-01517-y.

Supplementary information The online version contains supplementary material available at https://doi.org/10.1038/s41567-022-01517-y.

Correspondence and requests for materials should be addressed to Or Katz.

Peer review information *Nature Physics* thanks the anonymous reviewers for their contribution to the peer review of this work.

Reprints and permissions information is available at www.nature.com/reprints.

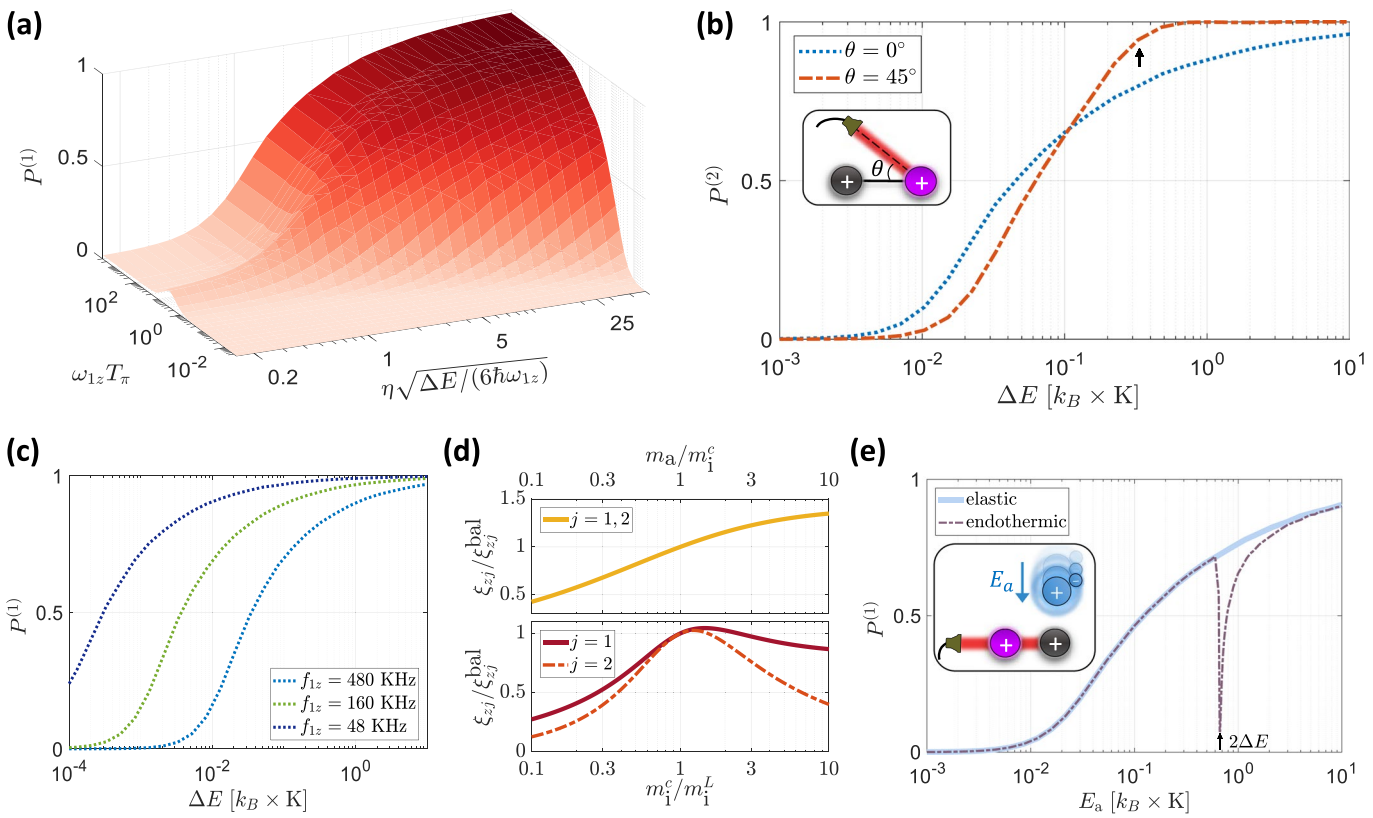

Extended Data Fig. 1 | Detection efficiency of electron shelving technique and its extension to additional configurations. (a) The probability $P^{(1)}$ to measure the ion in the S, electronic ground-state, (bright) after a single shelving π-pulse of duration T_π, following a single exothermic process releasing a total energy ΔE. For energetic processes ($\Delta E \gg \eta^2\hbar\omega_{1z}$) and low beam power ($\omega_{z1}T_\pi \gtrsim 1$) the detection of hot events approaches unity. Variation of the pulse duration T_π implies simultaneous change of the Rabi frequency and pulse duration. **(b)** Detection efficiency of two pulses of electron shelving in the low beam power limit with the experimental parameters. A tilted beam (red) features sharper detection curve with respect to a beam co-linear with the trap axis (blue, denoted as the 'base configuration' in this analysis) that is sensitive to motion only along that axis. Black arrow marks the energy of hyperfine-changing collision studied in the experimental realization. **(c)-(e)** Extensions of the base configuration. **(c)** Variation of the the axial trap frequency enables detection of exothermic processes releasing energy below $k_B \times$ (1 mK) at standard trap frequencies. **(d)** Configurations with unbalanced masses change the detection probability for exothermic process via scaling of the parameters ξ_{z1}, ξ_{z2} [c.f. Eq. (5)-(6))]. Top: variation of the atom to chemistry-ion mass ratio for a fixed $m_i^L = m_i^c$. Bottom: variation of the chemistry-ion to logic-ion mass ratio for a fixed m_i^L and $m_a = m_i^L$. **(e)**. Detection of elastic and endothermic collisional processes. An atom with kinetic energy E_a and moving perpendicular to the beam direction can scatter and generate motion of the crystal along the axis detected by the shelving beam (light-blue curve) in the base configuration. An endothermic process which converts a kinetic energy ΔE into internal one can be detected efficiently by varying the kinetic energy of the atom near $E_a = 2|\Delta E|$ (brown curve). Data in **(a)-(e)** is calculated numerically.